

Lawrence Berkeley National Laboratory

Recent Work

Title

FURTHER DEVELOPMENT OF A FACILITY FOR CHANNELING STUDIES: APPLICATION TO LATTICE LOCATION

Permalink

<https://escholarship.org/uc/item/2vq475fj>

Author

Lopes, D.R.

Publication Date

1984-08-01



Lawrence Berkeley Laboratory

UNIVERSITY OF CALIFORNIA

Materials & Molecular Research Division

FURTHER DEVELOPMENT OF A FACILITY FOR CHANNELING
STUDIES: APPLICATION TO LATTICE LOCATION

D.R. Lopes
(M.S. Thesis)

August 1984

RECEIVED
LAWRENCE
BERKELEY LABORATORY

SEP 10 1984

For Reference

Not to be taken from this room

LIBRARY AND
DOCUMENTS SECTION



LBL-18185
e.1

DISCLAIMER

This document was prepared as an account of work sponsored by the United States Government. While this document is believed to contain correct information, neither the United States Government nor any agency thereof, nor the Regents of the University of California, nor any of their employees, makes any warranty, express or implied, or assumes any legal responsibility for the accuracy, completeness, or usefulness of any information, apparatus, product, or process disclosed, or represents that its use would not infringe privately owned rights. Reference herein to any specific commercial product, process, or service by its trade name, trademark, manufacturer, or otherwise, does not necessarily constitute or imply its endorsement, recommendation, or favoring by the United States Government or any agency thereof, or the Regents of the University of California. The views and opinions of authors expressed herein do not necessarily state or reflect those of the United States Government or any agency thereof or the Regents of the University of California.

LBL-18185

FURTHER DEVELOPMENT OF A FACILITY FOR CHANNELING STUDIES:
APPLICATION TO LATTICE LOCATION

David Robert Lopes
M.S. Thesis

Lawrence Berkeley Laboratory
University of California
Berkeley, California 94720

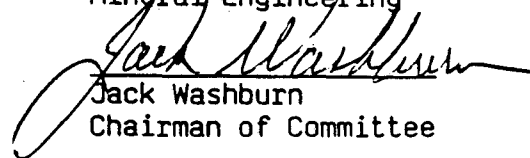
August 1984

Further Development of a Facility for Channeling Studies:
Application to Lattice Location

Master of Science

David Robert Lopes

Engineering Science:
Materials Science and
Mineral Engineering



Jack Washburn
Chairman of Committee

Abstract

Equipment modifications at the Lawrence Berkeley Laboratory (LBL) Rutherford backscattering facility, including the addition of a high precision goniometer, have been made to enhance the performance of channeling experiments. The angular divergence of the alpha particle beam was also reduced to $<0.05^\circ$ by improving the collimation. To demonstrate improved channeling capability angular scans were performed about the $\langle 100 \rangle$, $\langle 110 \rangle$, and $\langle 111 \rangle$ axial channels of a 3400 Å (100) silicon membrane. Both the minimum yield, χ_{\min} , and the critical angle, $\psi_{1/2}$, were consistent with accepted values. A preliminary investigation of the lattice location of cobalt on the (100) silicon surface was undertaken. Approximately 4.5×10^{15} Co atoms/cm² were electron beam deposited on a 3900 Å, HF etched silicon membrane in a system using oilless pumps. Preliminary channeling data taken approximately one month later indicated a preferred site for approximately 16% of the cobalt atoms. Channeling data obtained six months later with the new goniometer showed no evidence for a preferred site. Room temperature oxidation between experiments was observed and is thought to have affected the location of the cobalt atoms.

Acknowledgements

I am grateful to Professor Jack Washburn for his guidance, encouragement, and generosity of time. It has been a pleasure to work under his supervision and support. I am also thankful to Professor Nathan Cheung for his guidance, insight, and expertise in channeling. I appreciate Professor Eicke Weber's interest in this work and am thankful for his suggestions and participation on my thesis committee.

The LBL staff associated with the Rutherford scattering facility are Joe Jaklevic, Bill Searles, and graduate student Kin Man Yu. I am thankful for the part each of these individuals have played in the completion of this work. Kin deserves a special thanks for the many hours he has aided me in obtaining channeling data. Two other colleagues of mine, Gary Atkinson and Wing Leung, have provided valuable assistance in the preparation of the thin membranes used in this work.

My wife Laura deserves a special thanks for her excellent job of preparing the manuscript.

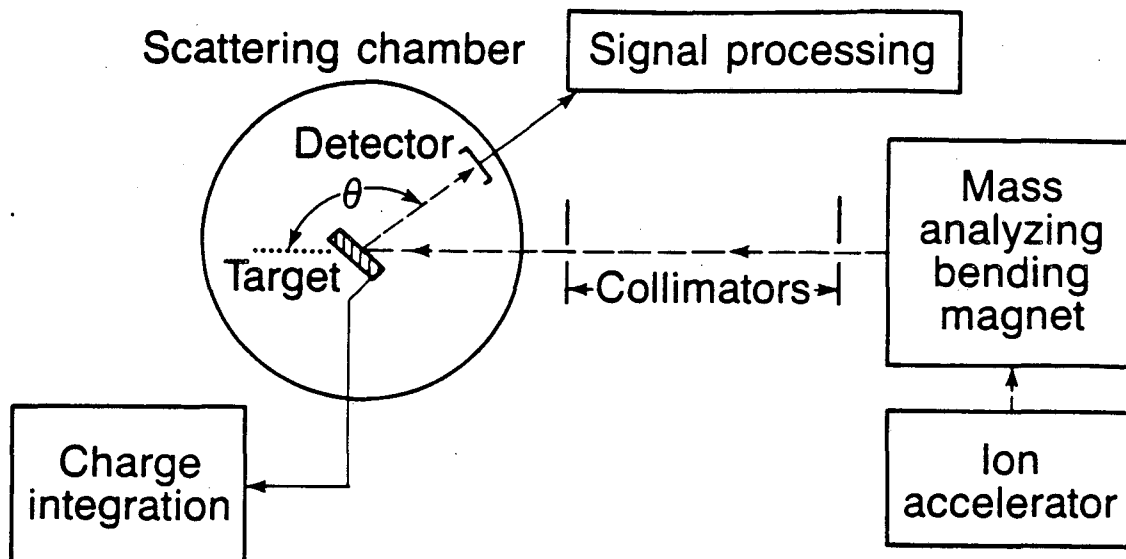
This work was supported by the Director, Office of Energy Research, Office of Basic Energy Sciences, Materials Science Division of the U.S. Department of Energy under Contract Number DE-AC03-76SF00098.

Table of Contents

	<u>Page</u>
1. Introduction	1
1.1 Fundamental Scattering Concepts	2
1.2 Channeling.	7
1.3 Lattice Location of Impurity Atoms in Bulk Crystals . .	11
2. The LBL Rutherford Backscattering Facility	18
2.1 Previous Experiments using Channeling	19
2.2 Improved Apparatus for Channeling	20
2.3 Demonstration of the Modifications.	25
3. Lattice Location of Cobalt	30
3.1 Lattice Location of Surface Atoms	32
3.2 Experimental.	34
3.3 Results	35
3.4 Discussion	42
4. Conclusions.	45
5. References	47

1. Introduction

Rutherford backscattering spectrometry (RBS) employs MeV ions to probe the near surface region of solids. In the usual energy range of 0.1 to 5 MeV, the light probing ions will create little damage to the sample and can provide quantitative information due to the well known scattering cross section and the empirical data on energy loss in solids. Applications include the measurement of the thickness and stoichiometry of thin films, the study of reaction kinetics of thin films, and the identification of surface elements. A schematic illustration of the components needed in an ion scattering experiment are pictured in Figure 1. A given ion specie, such as ${}^4\text{He}^+$, is accelerated and directed toward the scattering chamber by the accelerator and bending magnet. The ion beam is collimated after the bending magnet and enters the chamber striking the sample. As the helium ions penetrate the sample they lose energy via interaction with electrons. Most of the ions come to rest in the sample causing the sample to become charged. Actually the charge does not accumulate in the sample but is collected, thereby allowing one to determine how many ions have struck the sample. A small fraction of the helium ions undergo a large angle scattering event sending them back out of the crystal with a variety of energies depending on the scattering mass and the energy lost in the sample. The fraction of such backscattered ions falling within the solid angle of the detector are collected. The resulting charge in the detector is amplified and processed in the counting electronics. The resulting spectrum consists of a plot of the yield or number of detected



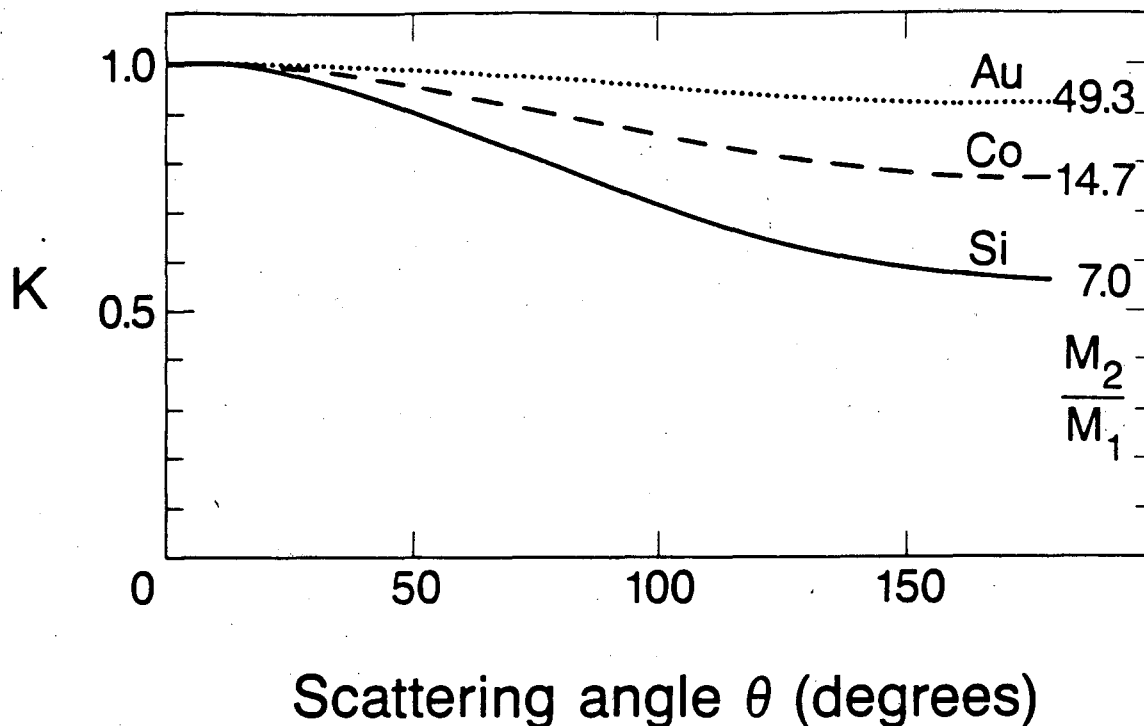
XBL 847-10734

Figure 1. Elements of an ion scattering facility.

ions vs. the energy of the ions. An example is given in the next section after the fundamental concepts of scattering are introduced.

1.1 Fundamental Scattering Concepts

There are three essential concepts necessary to understand a backscattering spectrum.¹ The kinematic factor gives the energy with which the ion recoils after a collision with a lattice atom. It is defined by the relationship $E_1 = KE_0$ where E_0 is the initial ion energy and E_1 is the ion energy after the scattering event. The interaction can be described by the elastic scattering of particles where the lattice atom is stationary with respect to the high velocity ion. Hence, the kinematic factor may be found from conservation of energy and momentum. It is a function of the scattering angle and the ratio of the ion and scattering atom masses. Figure 2 illustrates the



XBL 847-10736

Figure 2. Dependence of the kinematic factor on scattering angle and scattering atom/ion masses. M_1 for He = 4

dependence for some of the elements of interest in this study. The kinematic factor and thus the scattered energy is larger (at all scattering angles θ) for larger scattering atom masses. Thus, if one had a backscattering spectrum with a variety of peaks at different energies corresponding to elements at the surface of a sample, one could use the kinematic factor to match the peaks to the elements present. One can also see from Figure 2 that the resolution of masses will be maximized at a scattering angle as close to 180° as possible since the difference in the kinematic factor and hence, the difference in the scattered energy between masses is greatest there.

Whereas the kinematic factor describes the energy of the scattered ions, the scattering cross section describes how frequently a collision

occurs that results in a scattering event at an angle θ . Since the scattering cross section has the dimensions of area, one can picture each nucleus presenting an area $d\sigma/d\Omega$ to the beam of incident ions. To determine the scattering cross section, a model for the force acting during the elastic collision must be postulated. The Rutherford scattering cross section assumes a Coulombic interaction potential between two bare nuclei. This is appropriate for describing large angle scattering events in which the impact parameter is smaller than the radius of the inner shell electrons. Furthermore, for 1-2 MeV ${}^4\text{He}^+$ ions one need not worry about nuclear reactions which occur at higher energies. The differential scattering cross section under these conditions is given by:

$$\frac{d\sigma}{d\Omega} = \left(\frac{Z_1 Z_2 e^2}{4E} \right)^2 \frac{4}{\sin^4 \theta} \frac{[1 - ((M_1/M_2)\sin\theta)^2]^{1/2} + \cos\theta}{[1 - ((M_1/M_2)\sin\theta)^2]^{1/2}}$$

where Z refers to atomic number, M to mass, E to energy, θ to scattering angle, and the subscripts 1 and 2 refer to the incident ion and scattering atom, respectively. Knowing the scattering cross section enables one to convert spectral peak areas to areal densities (atoms/cm²) and to calculate atomic compositions from area and scattering cross section ratios.

Unlike the rare occurrence of a large angle nuclear interaction, ions are constantly losing their energy primarily through interactions with electrons of the target material. Since detected ions scatter from various depths within a sample, one must understand the energy loss of the ion into the material before the scattering event and the energy

loss out of the material before being detected. Theoretical models of energy loss (or dE/dx loss), although not capable of providing good numerical values, show that it depends on the incident energy of the ions as well as on the atomic density, atomic number, and other parameters of the scattering atom. These models, along with empirical data, provide energy loss values which have an accuracy of approximately 5%. For helium ions in the 1 MeV range, however, the energy loss is relatively independent of the ions' incident energy. This enables one to convert the energy scale of the backscattering spectrum to a depth scale rather easily. For example, if one assumes a constant value for dE/dx along the inward and outward paths (although not the same value!) one can easily write the relationship between the detected energy E_1 and the depth of scattering x as:

$$E_1(x) = KE_0 - \left[\frac{K}{\cos \theta_1} \frac{dE}{dx} \Big|_{in} + \frac{1}{\cos \theta_2} \frac{dE}{dx} \Big|_{out} \right] x$$

where θ_1 is the angle between the sample normal and the ion beam direction and θ_2 is the angle between the sample normal and the detector. This enables one to readily calculate the thickness of thin films with a depth resolution ranging from 30-200 Å depending on the values of θ_1 and θ_2 .

Figure 3 illustrates these fundamental scattering concepts. The backscattering spectrum consists of the yield or total number of detected counts plotted against the energy of the detected ion (sometimes expressed as the channel number of the multichannel analyzer). This spectra corresponds to a thin layer of barium fluoride on the back surface of a silicon membrane. It should be noted that the

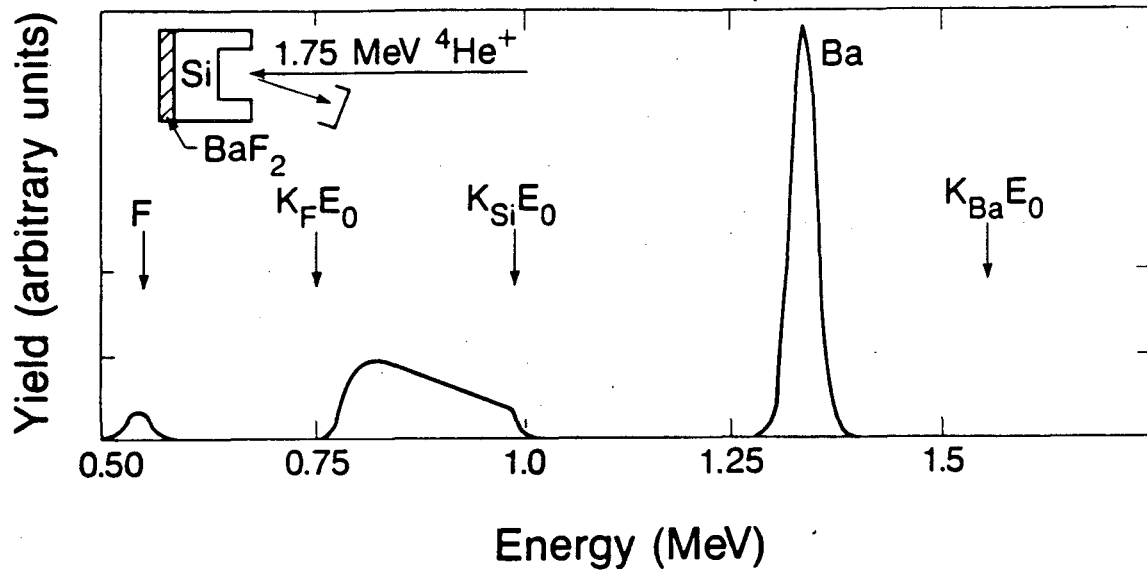


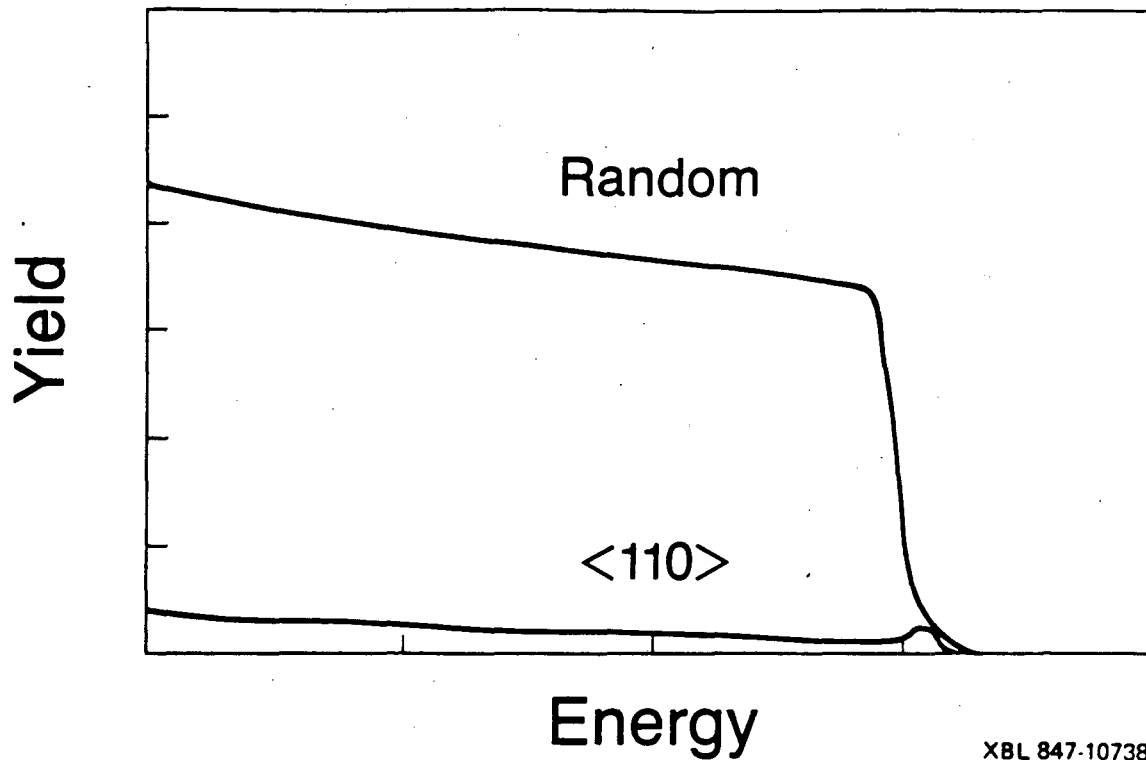
Figure 3. Example of a backscattering spectrum.

crystal is partially channeled (see next section) although that is not important in the present discussion. The high energy silicon edge is given by the kinematic factor. The barium and fluorine peaks shift to lower energies due to energy loss of the beam in the silicon. The thickness of the silicon membrane may be calculated either from the width of the silicon signal or from the shift in energy of the barium peak. Both calculations require knowledge of the energy loss behavior. The result is a thickness of 4300 ± 100 Å. Scattering cross section ratios are used to calculate the thickness of the BaF_2 layer (found to be ≈ 100 Å) and to verify that the layer is stoichiometric BaF_2 . Finally, the increase in yield of the silicon signal at lower energies is a general feature observed in backscattering spectra of thicker layers. It is due to the inverse relation of the scattering cross

section on energy. As the ions penetrate the sample they lose energy, the scattering cross section increases, and the yield increases.

1.2 Channeling

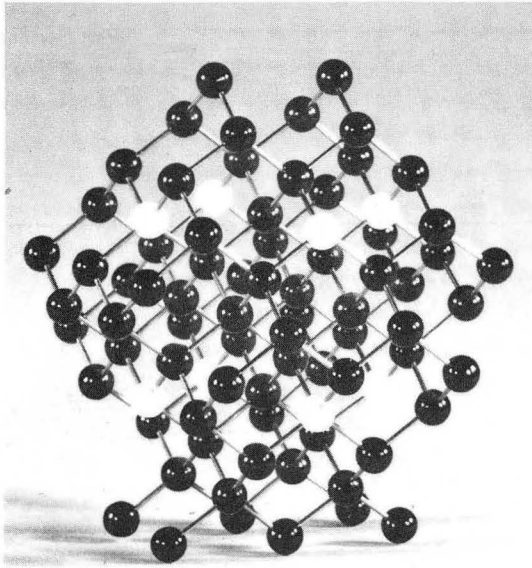
The backscattering spectrum from a single crystal randomly oriented with respect to the beam (or from an amorphous sample) differs greatly from that when the ion beam is aligned with a low index crystallographic direction of a single crystal.² Figure 4 shows the large decrease in yield and the small peak (called the surface peak) located at the high energy edge both characteristic of an aligned spectrum. Channeling is this orientational dependence of the yield. One might expect this type of behavior from an inspection of a ball and stick model of a crystal as in Figure 5. Channeling, however, in addition to a purely geometrical effect is more completely described by correlated small angle scattering events.³ In a randomly oriented crystal, as the incident ions penetrate deeper within the crystal, the flux distribution of the beam remains the same at each atom. In other words, the distribution of impact parameters of the ions is no different at one atom than another as a function of depth. Therefore, scattering events deeper within the crystal are uncorrelated with the scattering that has preceded it. Conversely, in the case of an aligned single crystal, the impact parameter distribution is uniform only at the uppermost atomic layer. At the surface (modeled by the abrupt termination of rows of atoms) more than 90% of the incident ions have impact parameters greater than 0.1 Å. At such distances the ions experience a screened Coulomb potential due



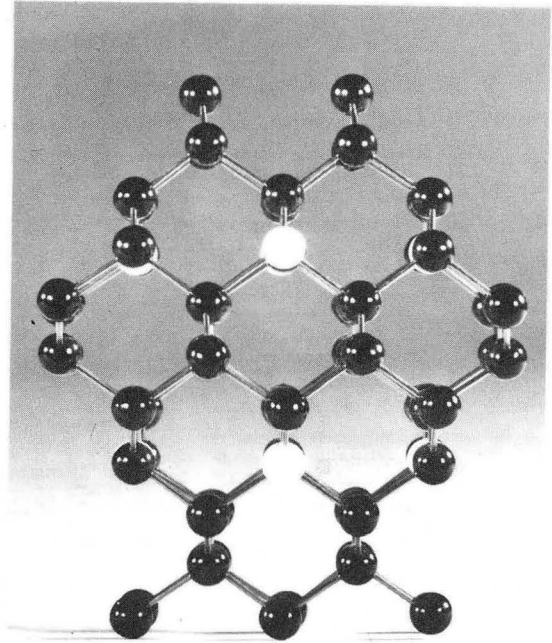
XBL 847-10738

Figure 4. Random and $\langle 110 \rangle$ channeling spectra.

to the electrons surrounding the nuclei and are scattered through small angles into the channel between the rows of atoms. The two uppermost atoms of one such row are pictured in Figure 6. The distribution of impact parameters at the second atom in the string is influenced by the small angle scattering events that take place at the first atom. Namely, a minimum impact parameter exists below which no ions can go. This was not the case at the first atom. At the second atom, another small angle scattering event occurs which influences the scattering at the third atom and so on. As the ion moves along the string of atoms it undergoes a gentle sequence of scattering events, steering it away from the string. The ion's trajectory oscillates between atomic rows with a wavelength of several hundred angstroms. The beam is at all



XBB 847-5125

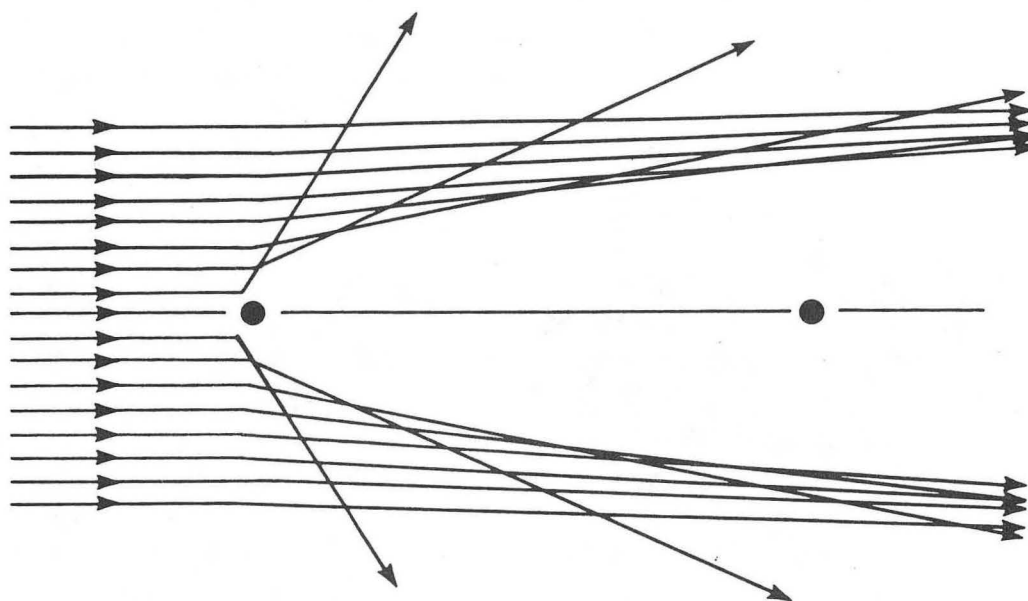


XBB 847-5124

Figure 5. Random and $\langle 110 \rangle$ axial channel direction in the diamond cubic structure.

times prohibited from occupying regions 0.1 \AA from the atom rows. This effect is called shadowing because subsequent atoms along a row are shadowed from the ion beam by the uppermost atoms. At depths of $0.1\text{-}1.0 \text{ \mu m}$ equilibrium is reached and the flux distribution is concentrated at the center of the channel. This is called flux peaking. In summary, channeling involves correlated small angle scattering events leading to a non uniform flux distribution.

Two other types of interactions at the surface of an aligned crystal should be mentioned. A small number of ions have impact parameters small enough to scatter through large angles. These ions give rise to the surface peak as seen in Figure 4. The remaining small fraction of the beam is scattered through large enough forward angles that they cannot be confined to the channels. This portion of the beam is called the random fraction.



XBL 847-10735

Figure 6. Two atom model showing formation of the shadow cone.

There are many applications of the channeling technique. Before discussing one particular application (the lattice location of impurity atoms) in detail, it would be profitable to mention other types of channeling studies. One important use of channeling is to analyze crystalline quality. Unlike the shadowed host atoms in a single crystal, the channeled fraction of the beam may interact with defects and amorphous regions within a crystal. These ions are scattered out of their channeled trajectories. Some of the ions will be scattered through large enough angles to be detected while others are scattered out of the channel through small forward angles. This latter occurrence is called dechanneling. The dechanneled ions can now interact with the host atoms as in a randomly aligned crystal, and the scattering yield increases dramatically. Damage due to ion implantation,

recrystallization after annealing, and the lattice matching quality of epitaxial systems are examples of this type of investigation.

Another set of applications involves analysis of either the surface peak or, in the case of interfacial phenomena, the interface peak. As was mentioned earlier, the surface peak arises from interaction of the ion beam with the surface in the case of an aligned single crystal. If one considers the surface to be distorted in some way relative to the structure of the bulk, then it follows that in different orientations the surface peak would reflect those changes. The same holds true at the interface between two crystals. The quantitative analysis of the interface peak allows for determination of the amount of disordered atoms. Hence, one example of its use would be in studying the reactivity of interfaces. Examples of surface investigations include reconstruction (displacement of atoms in the plane of the surface), relaxation (displacement of atoms normal to the surface), and adsorbate induced surface structures.

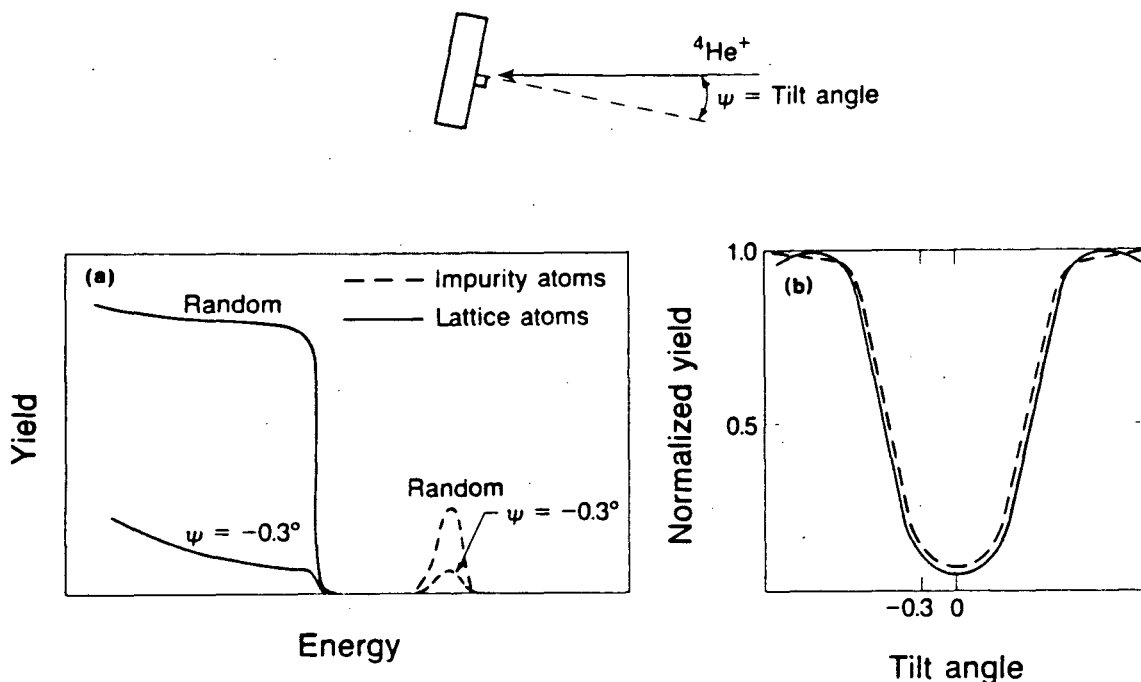
1.3 Lattice Location of Impurity Atoms in Bulk Crystals

The determination of the lattice location of impurity atoms with respect to the host lattice has been a popular application of the channeling technique. One reason for this is the critical importance that the location of impurities in solids have on structural, electrical, and optical characteristics. For example, studies on the substitutional fraction of dopants in semiconductors after ion implantation have been important in understanding electrical properties of these materials. Another reason is the scarcity of other techniques

which can supply this information. Channeling, however, has its limitations. It is best suited for studying impurities with high atomic numbers in samples of low atomic number. Furthermore, impurity concentrations in the range of $10^{19} - 10^{20}$ atoms/cm³ are necessary. It is important to realize that although the sensitivity for detecting elements is below this level, the beam damage associated with a lower concentration sample may be significant. For example, it has been shown that arsenic atoms in silicon can be displaced off substitutional sites with typical beam doses. Finally, it is possible to determine lattice locations as close as 0.1 Å to a substitutional site with an accuracy of 0.1 Å under favorable conditions.⁴

One begins a lattice location experiment by precisely aligning the crystal with the ion beam. This is usually done by tilting the crystal about 7° off axis and rotating through 360° while observing the count rate coming from the near surface area (~5000 Å) of the crystal. As planar channels are encountered the count rate drops off. The rotational position of the planar channels are recorded and a polar plot is generated. Additionally, the planar channels may be identified by the magnitude of the decrease in yield. The polar plot provides both the location of the axial channel and the crystallographic information necessary for tilting to other major crystallographic orientation. An example of a polar plot is shown in Figure 7 along with the stereographic projection for comparison.

Once the desired orientation is located, the lattice location experiment proceeds by monitoring the signals from the impurity and lattice location atoms as a function of tilt angle. Beginning at a tilt

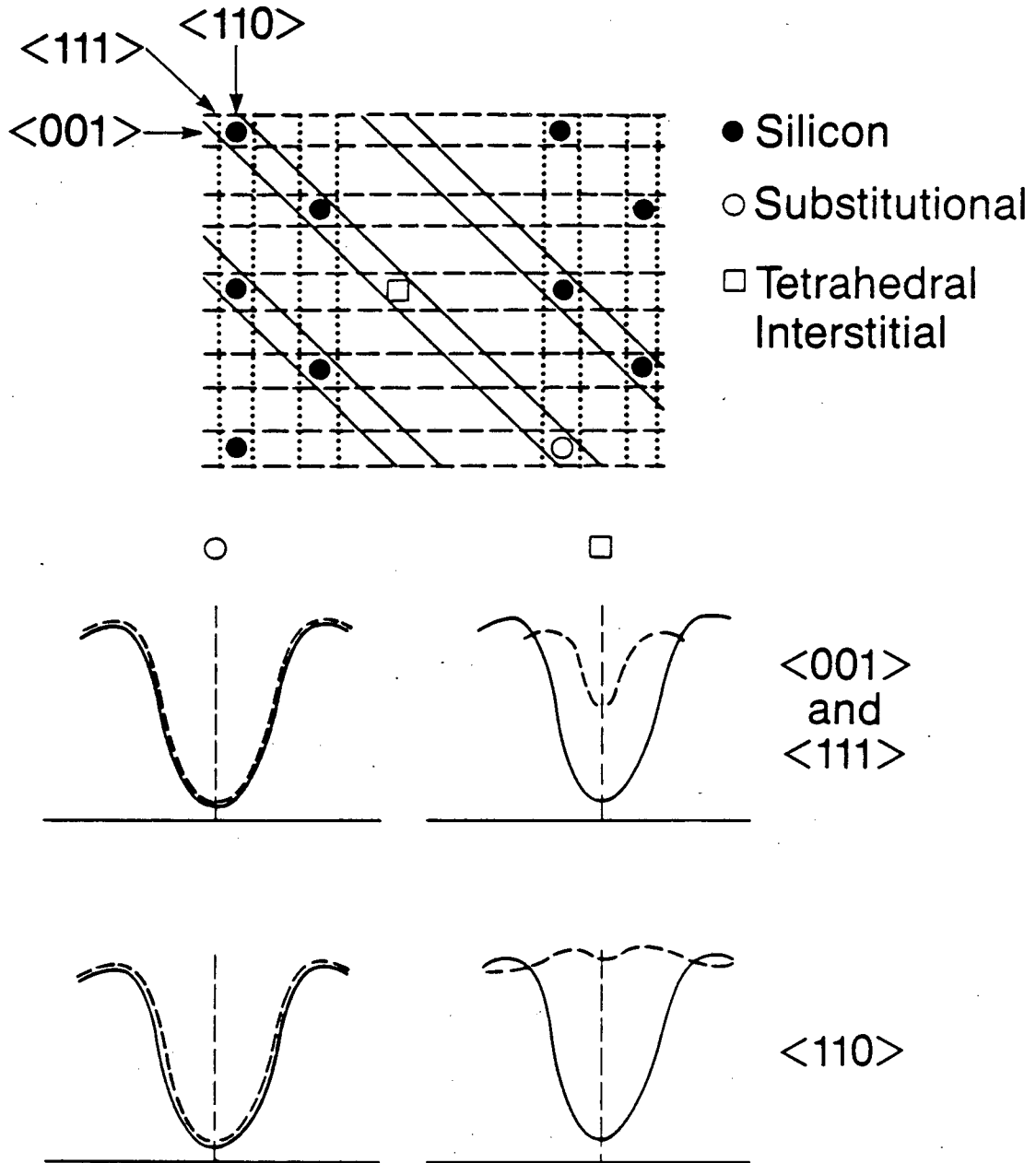


XBL 847 10746

Figure 8. Relationship between individual spectra and an angular scan.

individual energy spectra and the angular scan. Figure 8a shows two backscattering spectra, one at a random orientation and one 0.3° away from the aligned position. The data in Figure 8a provides one data point on each of the angular scans shown in Figure 8b. Two quantities characterize the angular scan: the minimum yield, χ_{\min} , and the half angle, $\psi_{\frac{1}{2}}$. The minimum yield is the normalized yield at 0.0° tilt and the half angle is the half width at half maximum of the dip. The half angle is a measure of the critical channeling angle which is the maximum incident angle for which incident particles are steered by the atomic rows into channeling trajectories. In the following discussion $\chi_{\frac{1}{2}}$ will be called the critical angle although it is to be understood that it is only a measure of it.

The shape of the angular scan and its importance in a lattice location experiment may be understood readily with reference to Figure 9. The {110} plane of the diamond cubic structure is pictured together with a substitutional and a tetrahedral interstitial impurity. Angular scans corresponding to three major crystallographic directions are shown. The dip characteristic of the lattice atoms results from shadowing. At small tilt angles the yield from lattice atoms is greatly reduced due to the channeling effect. As the tilt angle increases the atomic rows are imperfectly shadowed from the beam, and the yield increases. At angles of approximately 2° the ions have too great a transverse kinetic energy to become channeled at all and the yield corresponds to that of random orientation. Hence, in all major crystallographic directions the angular scan of the lattice atoms will have a similar appearance, with slight differences in χ_{\min} and $\psi_{1/2}$ depending on the orientation. Just like a lattice atom, substitutional atoms are shadowed at small tilt angles with a corresponding decrease in yield. Hence, the angular scan of a substitutional impurity shows a large dip similar to that of the lattice atoms in terms of both χ_{\min} and $\psi_{1/2}$ for all orientations. If all the impurity atoms occupy substitutional sites, then the angular scan will exactly match that of the lattice atoms. Next, consider the interstitial impurity. Along the $\langle 001 \rangle$ and $\langle 111 \rangle$ directions it is shadowed by the lattice atoms, and one sees a dip in the angular scan. The magnitude of the dip depends on the percentage of impurity atoms occupying this site. The width of the dip will be the same as for the host atoms if all the impurities are located exactly at the



XBL 847-10747

Figure 9. Angular scan for host, substitutional impurity, and tetrahedral interstitial impurity in the diamond cubic structure.

interstitial site. If a fraction of them are located just off the interstitial site, $\psi_{1/2}$ will be reduced. The interstitial position is not shadowed in the $\langle 110 \rangle$ direction. In this case no dip in the angular scan will be seen. In fact, due to a concentration of the particle flux toward the center of the channel, one often observes an increase in yield as shown in Figure 9. Therefore, it is possible to distinguish between impurities occupying substitutional sites and those located at interstitial positions by a qualitative comparison of angular scans about major axial channels. In the diamond cubic or zinc blende structures the angular scan about the $\langle 110 \rangle$ axial channel most readily distinguishes between the substitutional and interstitial site. This process of site differentiation by analyzing the results of angular scans about a variety of different crystallographic directions is called triangulation. Lattice site determination of more complex cases, such as nearly substitutional impurities, is aided by angular scans from many orientations including planar channels.

2. The LBL Rutherford Backscattering Facility

The Rutherford backscattering facility at the Lawrence Berkeley Laboratory (LBL) has previously been used for routine backscattering measurements such as characterization of thin films in terms of thickness and stoichiometry, as well as some channeling measurements. The facility uses a Van de Graaff accelerator to accelerate helium or occasionally hydrogen ions. Typically 1-2 MeV, singly charged helium ions are used in scattering experiments. The terminal voltage stability is ± 500 eV. A 90° bending magnet is used to separate the desired ionized specie from other unwanted beam components. Two more bending magnets route the alpha particles through the beam line to the scattering chamber. In previous experiments two collimators within the chamber limited the beam divergence to half angle of $\sim 1^\circ$. Samples are mounted to a goniometer which is controlled manually outside the chamber. A silicon surface barrier detector is typically mounted about 10 cm from the sample at a scattering angle of 170° . Inside the chamber there is a preamplifier. The rest of the counting electronics are outside the chamber. The output leads to a multichannel analyzer on which one sees the yield versus channel number spectra mentioned earlier.

The focus of this thesis is on the modifications to the apparatus such that channeling measurements may be done with more precision and more routinely. In this chapter previous channeling experiments will be discussed, the major improvements to the equipment will be described, and the enhanced channeling capability will be demonstrated. The following chapter will then describe a lattice location investigation.

2.1 Previous Experiments Using Channeling

Although channeling measurements have been made at LBL in the past, they have been quite limited. The prior experiments involve the characterization of damage structures which result from ion implantation⁵ or analysis of those which persist after thermal⁶ or laser annealing.⁷ In these experiments the channeling data has been used to show qualitative agreement with data obtained from transmission electron microscopy (TEM). Attempts were made to exploit the quantitative possibilities of RBS to measure the mean depth and width of damaged layers.⁵ The quantitative data gleaned from TEM was used as the standard by which various methods of interpreting the channeling data were judged. In another related experiment a qualitative investigation was made of the relationship between dechanneling and various damage structures.⁸ Three dimensional dislocation networks and fine point defect clusters were found to cause significant dechanneling while a sample with a density of $4.5 \times 10^{10} \text{ cm}^{-2}$ dislocation loops did not produce measurable amounts of dechanneling. Thus, previous use of the channeling facility did not involve:

- alignment along other axial or planar channeling directions than the cut orientation of the crystal
- small, precise tilt movements about a channeling direction, as in an angular scan
- a calibrated system capable of giving quantitative information such as the areal density corresponding to a peak in the spectrum

Although one would not expect investigations of disorder to involve the later two elements, it is surprising that other orientations, particularly planar directions, were not attempted. Picraux, et al.⁹ has suggested that planar channeling might be more useful in determining the depth distribution of dislocations than axial channeling. This is due to the fact that the dechanneling cross section, σ_D , for point defects and dislocations is a function of $\psi_{\frac{1}{2}}$.¹⁰ In particular, $\sigma_D \sim \psi_{\frac{1}{2}}^{-1}$ for dislocations. Hence, the relative increase in the channeling yield from the planar orientation will be greater than that of the axial case because $\psi_{\frac{1}{2}}$ is smaller for planar orientations. Nevertheless, the central point of this section is that up until now the channeling experiments at LBL have been limited to alignment along the cut orientation of a crystal.

2.2 Improved Apparatus for Channeling

There are two essential components for channeling measurements. The most important piece of equipment is a high precision goniometer (sample manipulator). The goniometer should have at least three axes: two for angular rotations and one for translation. The axes of rotation may either be both perpendicular to the beam, as well as being mutually orthogonal, or one of the rotational axes may be parallel to the beam. In the later case, the rotational movement about the beam axis must be capable of rotating 360°. The rotational movements with axes perpendicular to the beam must be able to tilt far enough that all desired orientations may be obtained. Hence, one would usually want the extent of tilt to be approximately 60°. The precision of the rotational

movements must be $<0.05^\circ$. Performing an angular scan is the most demanding type of channeling measurement. One is often interested in taking data at 0.1° intervals. However, at orientations off the cut orientation of the crystal, angular scans are combinations of both rotational movements. Hence, it is often the case that to move a 0.1° increment, an individual rotational axis will be moved 0.07° . The necessary feature of a goniometer is that it must be able to rotate the sample in a single direction in precise steps, each step being the same magnitude as the last. Therefore, the absolute accuracy of the movement is not so much of a concern as is its linearity. If one thinks that one is stepping by 0.1° increments when actually the increments are only 0.09° , the error can be easily detected and compensated for with reference to a known value of $\psi_{\frac{1}{2}}$, for example. However, if while stepping by 0.1° increments one was moving sometimes by 0.05° and other times by 0.15° , then uncertainty due to nonlinearity is introduced which cannot be corrected for. So it is important to have as high a readout resolution as possible ($\sim 0.01^\circ$) and a precision of movement which certainly must be $<0.05^\circ$ and more on the order of 0.02° . Translation is important for moving the beam spot to different areas on the sample. It is possible to do this in some systems by steering the beam instead of translating the sample, in which case only a two axis goniometer is required. Assuming one needs a translation stage, its most important feature is that its motion be uncoupled to the rotational movements, such that when the sample is translated no change in orientation of the sample occurs. Likewise, the two rotational motions should not be coupled. Although in principle coupled motions could be compensated for

once they were adequately characterized, it would be very difficult to perform an angular scan away from the cut orientation (where both rotational movements are being incremented by small amounts) due to backlash error. Other desirable features of the goniometer include a design which allows one to detect particles scattered at grazing angles (just greater than 90°) and second, to detect transmitted particles (say at $\theta = 70^\circ$) in the case of thin crystal samples. The former case is useful in applications where maximum depth resolution is required while the latter is essential for transmission channeling experiments.

In past years a modified X-ray diffraction goniometer was used for channeling experiments. It had five axes of movement including two translational motions and three rotational movements. The rotational axis coincident with the beam could rotate at least 360° . Of the other two axes one was capable of tilting approximately 55° while the other was restricted to about 30° . The precision of the rotational movements was reported to be $\pm 0.05^\circ$ and to be independent. However, at the time of this investigation the rotational motion whose axis parallels the beam was found to be coupled to the other rotational movements. Furthermore, its precision was much worse than $\pm 0.05^\circ$. The state of the goniometer could not be brought back to the original specifications. In summary, this goniometer could be used to align crystals at the cut orientation and perform an angular scan, but angular scans at tilted orientations were not possible to obtain. Further, the design of the goniometer allowed for neither grazing exit angle measurements nor for transmission scattering experiments.

For these reasons a three axis, high precision goniometer was acquired from Custom Goniometer Systems. The goniometer is configured with two rotational motions, one whose axis is parallel to the beam, and one translational motion. The two rotational motions rotate continuously beyond 360° . The readout resolution of the rotational axes is 0.01° and their precision is much better than 0.05° . Also the backlash error ($\sim 0.1^\circ$) is much smaller than that of the previous goniometer. Most importantly, the three axes are independent. These features allow one to carry out channeling angular scans at any desired orientation. Furthermore, the sample mounting area is designed such that both grazing angle detection and transmission measurements are feasible. Although these features were not used in the present work they add important flexibility to the system for future work.

At the beginning of the section it was mentioned that channeling measurements involved two important components--the second is beam collimation. Poor beam collimation causes an increase in the yield at channeling orientations due to increased dechanneling. One may estimate the magnitude of this effect by examining an angular scan as in Figure 9. If one likens a divergent beam to a crystal slightly misoriented with respect to the beam, one sees that a beam divergence of $\sim 0.25^\circ$ causes a factor of two increase in yield. The increase in yield will actually be smaller since this estimate assumes all particles are misoriented rather than a fraction of them as in a divergent beam. A beam divergence of $\sim 0.05^\circ$ is usually considered a good compromise between the benefit in decreasing beam divergence and the accompanying decrease in beam current on the sample.

Prior to the present work, all collimation was done within the scattering chamber. With this arrangement the beam divergence could be limited to a half angle of $\sim 1^\circ$. It may be the case that the beam divergence was limited by other aspects of the beam steering and focusing system since reasonable values of χ_{\min} could be obtained. Nevertheless, these conditions might change from one run to another depending on the operating variables such as the beam energy, the beam focus, and the settings of the various bending magnets. For the sake of accuracy and consistency an upstream collimator was installed and aligned. Due to the limited amount of beamline between the last switching magnet and the scattering chamber, the second collimator had to be placed within the chamber. The collimators provide a half divergence angle of $\leq 0.05^\circ$ and limit the beam size to a diameter of 0.75 mm.

Another useful modification to the system was the addition of a single channel analyzer (SCA) to the counting electronics. The SCA allows one to monitor the yield from just the surface portion of the spectrum. This signal was then fed to the existing ratemeter with its recorder output driving a meter readout near the goniometer. This was useful in obtaining polar plots since the decrease in yield associated with the planar channels was much more apparent when only this portion of the spectrum was monitored. It is dechanneling that causes the yield to increase at greater depths, making the signal less sensitive to orientation effects.

A new secondary electron suppression system was also developed. It was previously described how the beam current is monitored by collecting

current from the sample. One of the largest sources of error in this measurement results when secondary electrons are ejected from the sample. If these electrons do not return to the sample, it appears that more helium atoms have struck the sample than actually have. Hence, some system of causing these electrons to return to the sample must be devised. Work began before the new goniometer arrived in order to increase the consistency of our measurements. Originally a magnetic faraday cup arrangement was used. This system was replaced by a cylinder biased to -900V surrounding the goniometer to repel the electrons back to the sample or goniometer. More consistent scattering yields were obtained by this method. When the new goniometer arrived a similar electrostatic suppression system was implemented.

Finally, the layout of the scattering chamber was completely reworked to allow for greater flexibility and accuracy in the positioning of detectors and other components. Furthermore, the entire base plate was made electrically isolated from the rest of the chamber to eliminate ground loops.

2.3 Demonstration of the Modifications: Silicon Angular Scans

To show the improved capacity of the LBL Van de Graaff facility for doing channeling experiments, angular scans about the $\langle 100 \rangle$, $\langle 110 \rangle$, and $\langle 111 \rangle$ directions of thin (100) silicon membranes were performed. This is an appropriate demonstration since it involves alignment at orientations other than the cut orientation of the crystal, precision tilting about each of these axes, and allows for comparison with known results. It should be emphasized that the angular scans at the $\langle 110 \rangle$

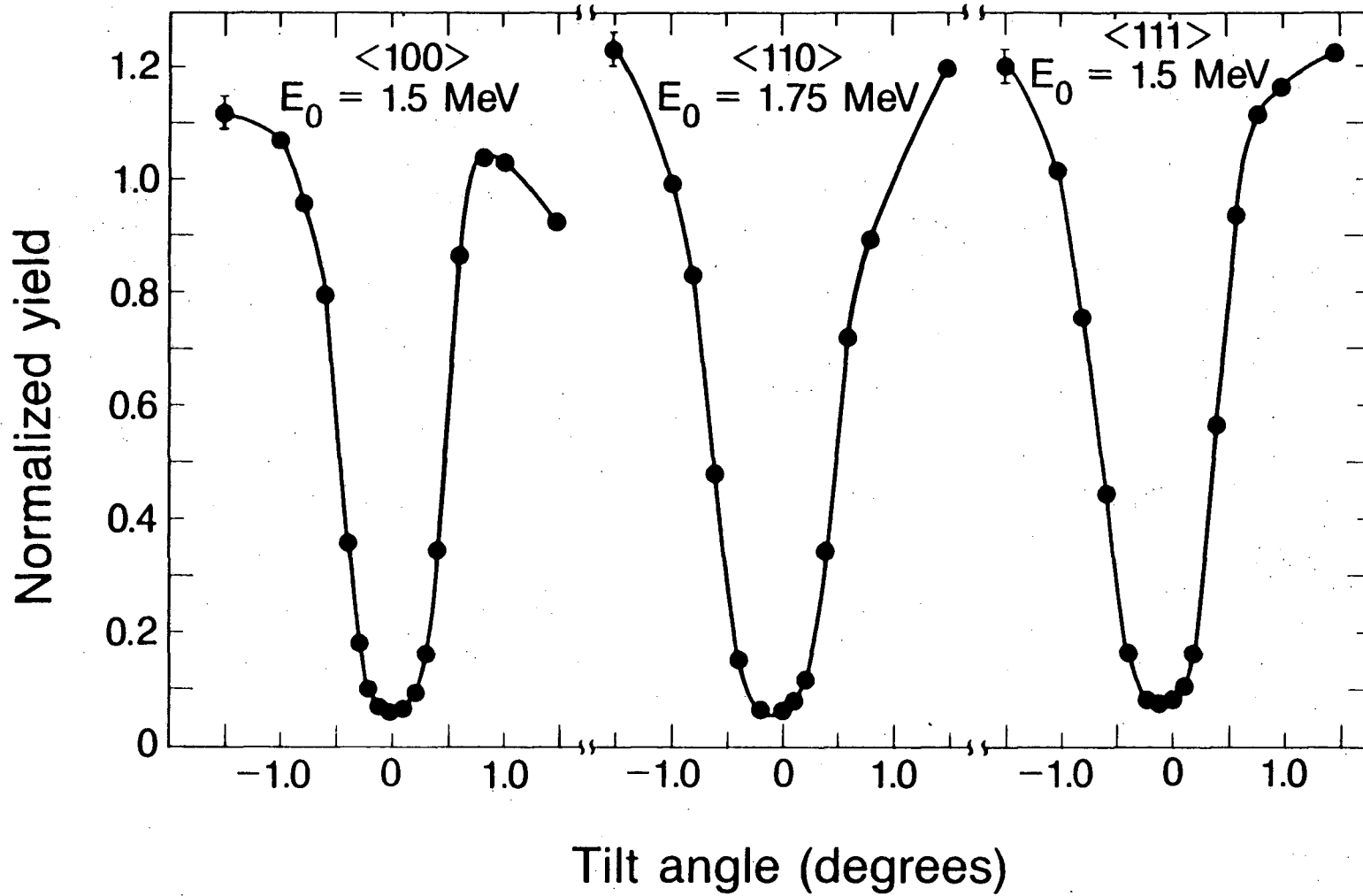
and $\langle 111 \rangle$ orientations are particularly meaningful since each increment of tilt involves a combination of movements of both rotational axes. This is in contrast to the $\langle 100 \rangle$ angular scan which is executed using only the rotational movement whose axis is perpendicular to the beam. The angular scans are shown in Figure 10 and the values of χ_{\min} and $\psi_{\frac{1}{2}}$ which characterize them are given in Table 1. In all cases care was taken in choosing the scan direction to avoid planar channels. The silicon signal was taken from the upper 1000 Å or less of the membrane. The values of χ_{\min} and $\psi_{\frac{1}{2}}$ may be compared with those calculated from the following expressions which are empirical fits to computer simulations.¹¹ The axial critical angle is given by:¹²

$$\psi_{\frac{1}{2}} = 0.8 F_{RS} (1.2 u_1/a) 0.307 (Z_1 Z_2/Ed)^{\frac{1}{2}}$$

where F_{RS} is proportional to the square root of the continuum Moliere potential, u_1 is the one dimensional rms vibrational amplitude, a is the Thomas-Fermi screening radius, E is the ion energy (in MeV), and d is the atomic spacing along the axial direction (in Å). The axial minimum yield is given by:¹²

$$\chi_{\min} = 18.8 N d u_1^2 [1 + (\psi_{\frac{1}{2}} d / 126 u_1)^2]^{\frac{1}{2}}$$

where N is the atomic density. The results of these expressions are compared with the experimental data in Table 1, which also gives the results on a $\langle 110 \rangle$ angular scan at 1.5 MeV which is not shown in Figure 10.



XBL 847-10739

Figure 10. <100>, <110>, and <111> silicon angular scans.

	E(MeV)	$\psi_{1/2}$		χ_{\min}	
		<u>Experimental</u>	<u>Accepted Value</u>	<u>Experimental</u>	<u>Accepted Value</u>
<100>	1.5	0.48	0.50	0.059*	0.030
<110>	1.5	0.63	0.61	0.056†	0.021
<110>	1.75	0.56	0.55	0.057**	0.021
<111>	1.5	0.53	0.53	0.074††	0.026

* $\chi_{\min} = 0.038$ at an undamaged position, and after background subtraction $\chi_{\min} = .031$.

** $\chi_{\min} = 0.038$ at an undamaged position, and after background subtraction $\chi_{\min} = .030$.

† $\chi_{\min} = .048$ after background subtraction

†† $\chi_{\min} = .059$ after background subtraction

Table 1

The comparison of experimental and accepted values is very good for the critical channeling angle. The values for χ_{\min} were uniformly higher than expected. There are two reasons why this occurred. In a prior experiment some discontinuities in the angular scan were introduced when the sample was translated. In these measurements a trade-off was made to remain at one spot on the sample in order to obtain a smooth, continuous angular scan. Beam damage of the sample was partially responsible for the inflated χ_{\min} values. In two cases an aligned spectrum was obtained at an undamaged position. The minimum yield was in much better agreement in these cases as shown in Table 1. The other contributing factor was background counts from an unknown source which grew larger as energy decreased. An estimate of the background was obtained for all cases. Background subtraction led to a significant decrease in χ_{\min} , although this correction is not as large as that due to beam damage. In summary, it has been demonstrated that it is possible to align single crystals at a variety of orientations and perform accurate angular scans.

3. Lattice Location of Cobalt

Much is known about the behavior of transition metals in bulk silicon including their location.³¹ These elements diffuse interstitially in silicon at elevated temperatures with high diffusivities. Both Electron Paramagnetic Resonance (EPR) and Mossbauer Spectroscopy show that upon quenching to room temperature Co, Ni and Cu atoms do not remain in unperturbed interstitial sites. The interstitial cobalt atoms form complexes or precipitate out.^{32,33} A small amount of substitutional Co forms when interstitial Co reacts with Si vacancies. This is valuable background information for the following study of cobalt located at the Co-Si interface.

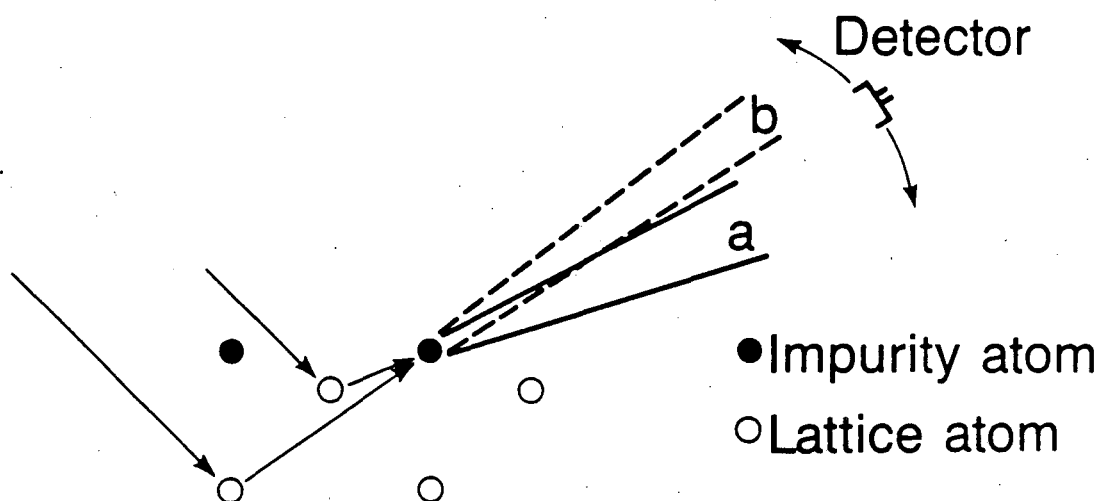
The increasingly demanding requirements of integrated circuit technology has resulted in a great deal of study of metal-silicon interactions. Examples include the interest in lower resistivity gate metallization (to minimize RC delay as linewidths are decreased) and the fabrication of reliable ohmic and rectifying contacts. Silicides (metal-silicon compounds) have many desirable properties including low resistivity, high temperature stability, and high resistance to electromigration.¹³ Two areas of ongoing inquiry are the prediction of Schottky barrier height^{14,15} and of the first silicide compound to form.¹⁶ For both of these questions a more detailed description of the metal-silicon or silicide-silicon interface is desired. Recently the importance of an interfacial layer has been postulated by various investigators. Experimental evidence for the existence of an interface layer is difficult to obtain. Ottaviani et al.¹⁷ have proposed that the interfacial layer will control Schottky barrier height, ϕ_b . To

demonstrate this they discuss a correlation between ϕ_b and the eutectic temperature which is considered to be an interfacial property exhibiting the influence of the interfacial layer. They were not able to define the extent, structure, or composition of the layer. Tu¹⁸ has proposed a mechanism to explain the low temperature (100-200°C) reaction between silicon and near noble metals consisting of interstitial metal atoms in the silicon crystal. The interstitial atoms transform the silicon covalent bonds at the interface to metallic bonds, and high interface mobility may be achieved. The region of near noble metal interstitial atoms in silicon may be considered as a model of the interfacial layer. The work of Cheung and Mayer¹⁹ has provided experimental evidence for such a model in the case of the Ni-Si interface. Walser and Bené²⁰ have discussed a method predicting the first compound to nucleate based on the existence of a glassy or amorphous interfacial layer. Bené et al.²¹ have presented evidence for the existence of this glassy layer for the Co-Si system.

The investigation presented here was undertaken to see if further information on the Co-Si interface could be obtained by studying the lattice location of cobalt on the silicon (100) surface. Experimental data was obtained both before and after the new goniometer was added to the system. The differences between this type of lattice location study and that of impurities located in bulk samples will be discussed in the next section.

3.1 Lattice Location of Surface Atoms

The techniques previously described for a lattice location study are not applicable to studying surface impurities on a thick crystal. The beam would encounter the surface atoms first, obviously, before any type of channeling effect of the beam could take place. The establishment of shadowed regions has been discussed as a necessity for lattice location experiments. Nevertheless, there are two methods that can be used to determine the lattice sites of impurity atoms at the surface. Van Der Veen et al.²² have described a technique which is capable of investigating monolayer or submonolayer impurity coverages on thick samples. The technique uses ions accelerated in the medium energy range ($50 < E_0 < 200$ keV) which are incident along channeling directions of the crystal and a movable detector which can be brought into alignment with the channeling directions of the crystal as well. Figure 11 gives an example of the side view of the surface region with a fraction of a monolayer of impurity atoms present. Of interest is how the surface scattering of the host atoms is shadowed by the impurity atoms. The shadow cone denoted "a" results from the shadowing of the surface scattering from the first host atom in the string while the cone marked "b" results from scattering from the second atom along the row. The characteristic of an angular scan (meaning in this context moving the detector, thereby changing the scattering angle) is the reduction in yield which occurs when the detector is aligned with the shadow cone radius. In the same manner as was previously described, triangulation is used to identify the impurity site. Monte Carlo computer simulations can be used to generate angular scans for comparison to the



XBL 847-10737

Figure 11. Scattering geometry for surface studies by double alignment.

experimental data to test various possible locations. Other than the equipment needed to perform this type of experiment (ultrahigh vacuum, electrostatic or magnetic analyzer for better resolution, etc.), it is important to realize that this type of experiment is not applicable to impurity coverages greater than one monolayer since a well defined shadow cone is required.

An alternative method of investigating the lattice location of surface atoms (and the one used in this study) involves the use of membranes several thousand angstroms thick.¹⁹ The beam is incident on the impurity free side first. As the beam penetrates through the membrane flux peaking is established. It then interacts with the impurity atoms on the back side of the membrane, is scattered back through the membrane, and is detected. Hence, the principles for this

experiment are the same as for a bulk location study. The only difference is the experimental detail of using a membrane thin enough that the beam can penetrate through it and the scattered particles return back out to the detector. For this type of experiment it is possible to use more than a monolayer of impurity atom coverage. One must be aware though, that as the impurity coverage increases the portion of the signal corresponding to atoms occupying preferred sites at the surface diminishes. Hence, there is an upper limit to the impurity layer thickness.

3.2 Experimental

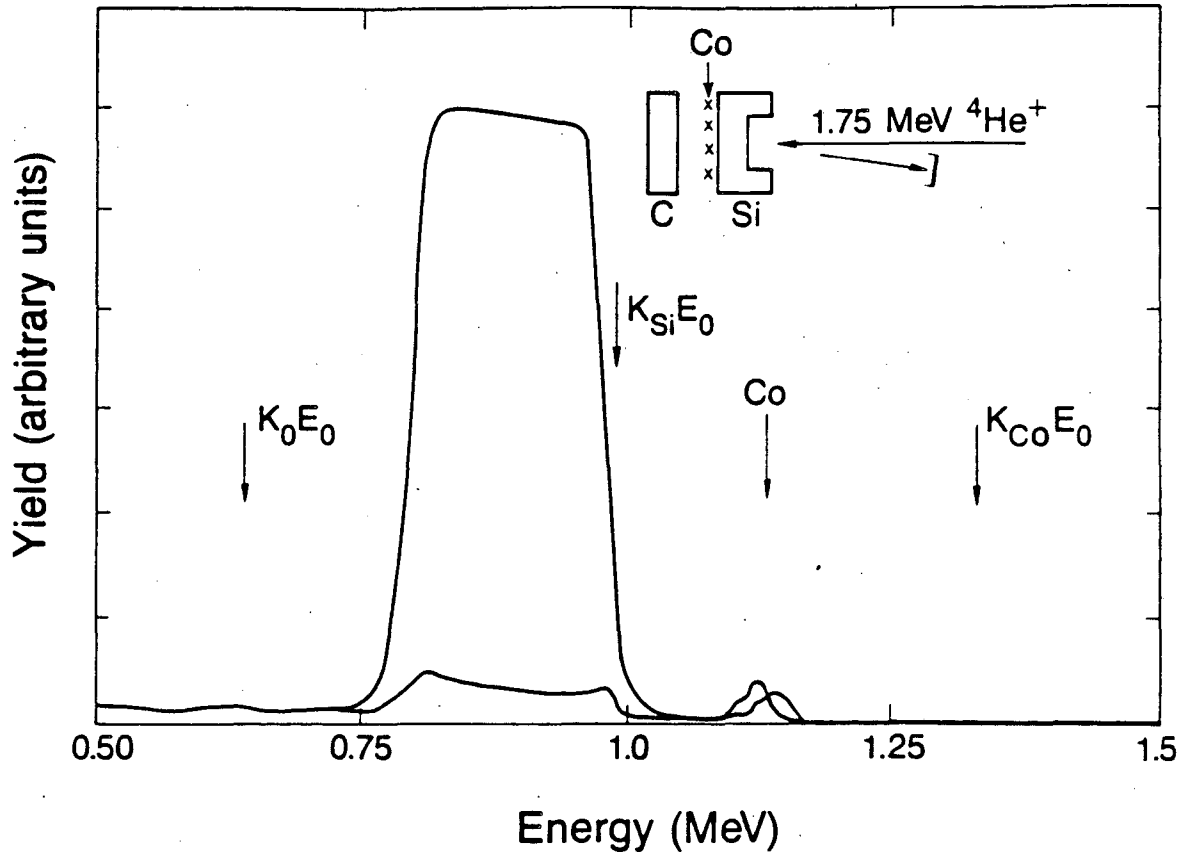
Thin silicon membranes were provided by Nathan Cheung of the Electrical Engineering and Computer Science department, U.C. Berkeley and prepared by Gary Atkinson. The basic process for making these samples has been reported in the literature.²³ The key step in the process is the use of a selective etchant, ethylenediamine-pyrocatechol (EDP) which does not attack silicon when doped with boron to a level exceeding 7×10^{19} atoms/cm³. Hence, one diffuses boron into an n- or p-type device grade silicon wafer such that this doping level reaches a depth corresponding to the desired membrane thickness. The wafer is then etched away from the backside and will stop upon reaching the boron doped region.

The cobalt deposition was done in an electron beam evaporator which uses only oilless pumps: a carbon vane pump, cryogenic pumps, titanium filament, and an ion pump. This is important in minimizing the amount of surface impurities on the membrane prior to evaporation. The

membrane was organically degreased and dipped in concentrated hydrofluoric acid just before loading into the evaporator. This procedure will leave $\leq 1 \times 10^{15}$ oxygen atoms/cm² and $\leq 5 \times 10^{14}$ carbon atoms/cm² on the silicon surface.¹⁹ The system was evacuated to 3×10^{-7} Torr prior to the deposition. In a previous study of the Ni-Si system^{19,26} it was found that a 10 Å coverage was a good compromise between the amount of impurity atoms necessary to initiate an interfacial reaction and that amount which would contribute a large random component to the impurity signal. Since the system was not equipped with a crystal monitor, calibration runs were done to determine the dependence of cobalt thickness on the length of time the shutter was opened at a given emission current. The needed deposition parameters were determined by extrapolating to lower thicknesses. The obvious uncertainties in such a procedure are the reason that, although a 10 Å coverage was desired, the actual thickness was close to 5 Å.

3.3 Results

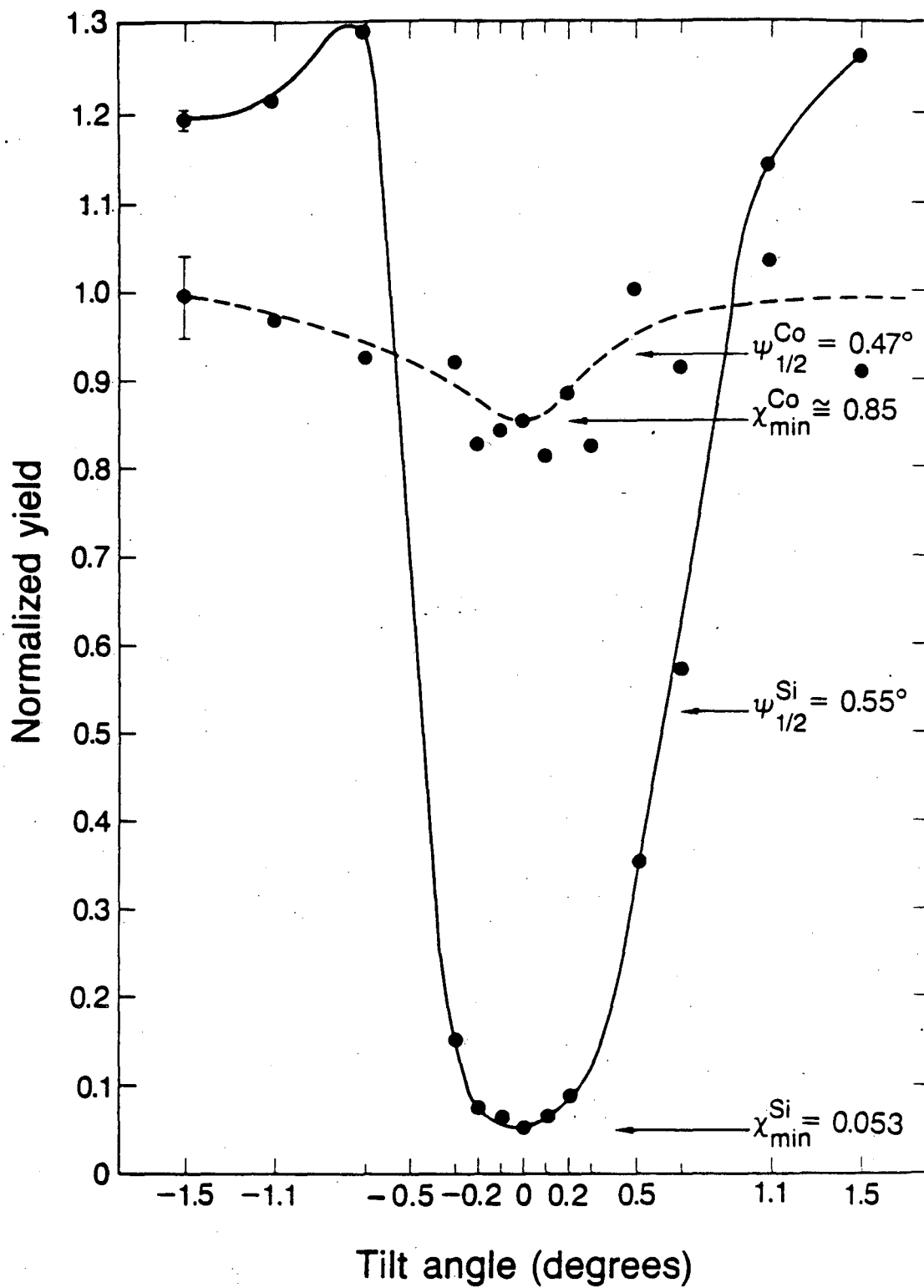
After deposition the sample was stored at room temperature for one month before preliminary tests could be performed using the old goniometer. Figure 12 shows random and $\langle 100 \rangle$ channeled spectra, as well as the scattering geometry. The helium ions were accelerated to 1.75 MeV, the scattering angle was 170°, and a beam dose of 3 μC was collected for each spectrum. Due to the limitations of this goniometer it was only possible to obtain an angular scan in the $\langle 100 \rangle$ channeling direction. The angular scan is shown in Figure 13. The silicon scan is obviously unsymmetric which leads to a discrepancy between the measured



XBL 847-10743

Figure 12. Random and $\langle 100 \rangle$ spectra showing silicon and cobalt.

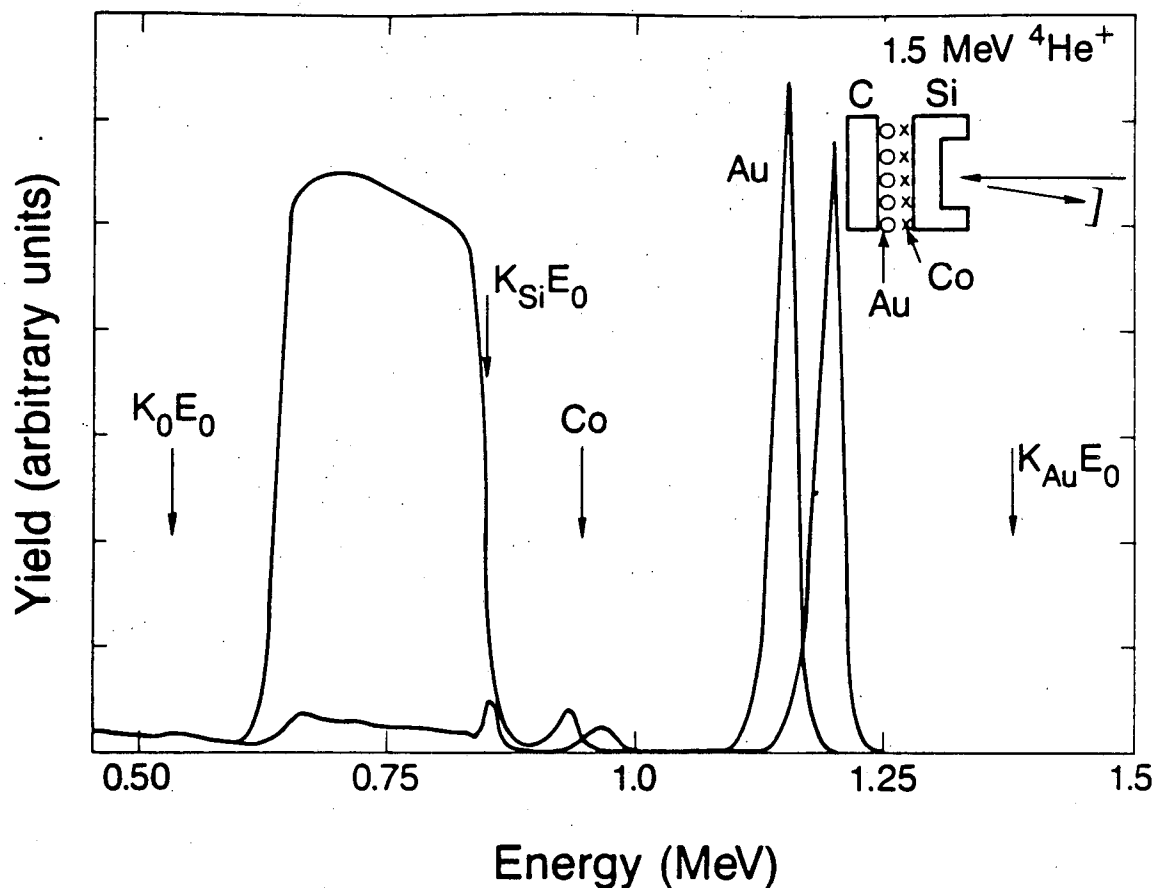
valve of the half angle of 0.55° and the known value of 0.46° . The minimum yield of 0.053 was significantly larger than the known value of 0.030 although it is plausible that this is due to beam damage which occurred during alignment. The cobalt curve, although showing a considerable amount of scatter due to the low count rate, indicated a slight dip which coincided with that of the silicon scan. The minimum yield may be estimated as 0.85 or a 15% decrease in yield while $\psi_{1/2}$ may be estimated as 0.47° . The uncertainty of an individual measurement due to counting statistics is shown in the figure, and according to that estimate of error the magnitude of the dip is statistically significant.



XBL 847-10740

Figure 13. Cobalt on silicon: <100> angular scan.

Six months after this data was taken the sample was tested again with the new goniometer. An aligned spectrum along the $\langle 100 \rangle$ channeling direction is shown with a random spectrum in Figure 14. The beam energy in this experiment was 1.5 MeV and a dose of 8 μC was used for each spectrum. One addition to the previous experimental set-up was a thin gold layer present on the carbon surface. This is useful for two purposes: first, to normalize fluctuations in charge integration and second, to normalize the anomolous difference in energy loss when the beam is aligned in a channeling direction compared to a random orientation. When the beam is channeled the energy loss is slightly less than if it were randomly oriented. Since the scattering cross section is inversely proportional to E^2 , the cobalt yield will be slightly reduced. Since the gold atoms are exposed to the same beam condition as the cobalt atoms, the change in the gold yield can be used to normalize the cobalt yield. The $\langle 100 \rangle$ angular scan is shown in Figure 15. The scan is much more symmetric. The half angle is 0.48° which compares well with the known value of 0.50° . Again χ_{\min} is somewhat higher than the known value due to beam damage. Most importantly, however, the cobalt yield shows no dependence on tilt angle indicating that it is randomly located at the silicon surface. One can clearly see that the scattering of the data points is of the same order as the uncertainty associated with the counting statistics. It is known that in some systems the beam can cause movement of the impurity atoms off preferred sites.²⁴ A beam effect has been observed in the Co-Si system.²⁵ So, to determine if this was a problem the sample was

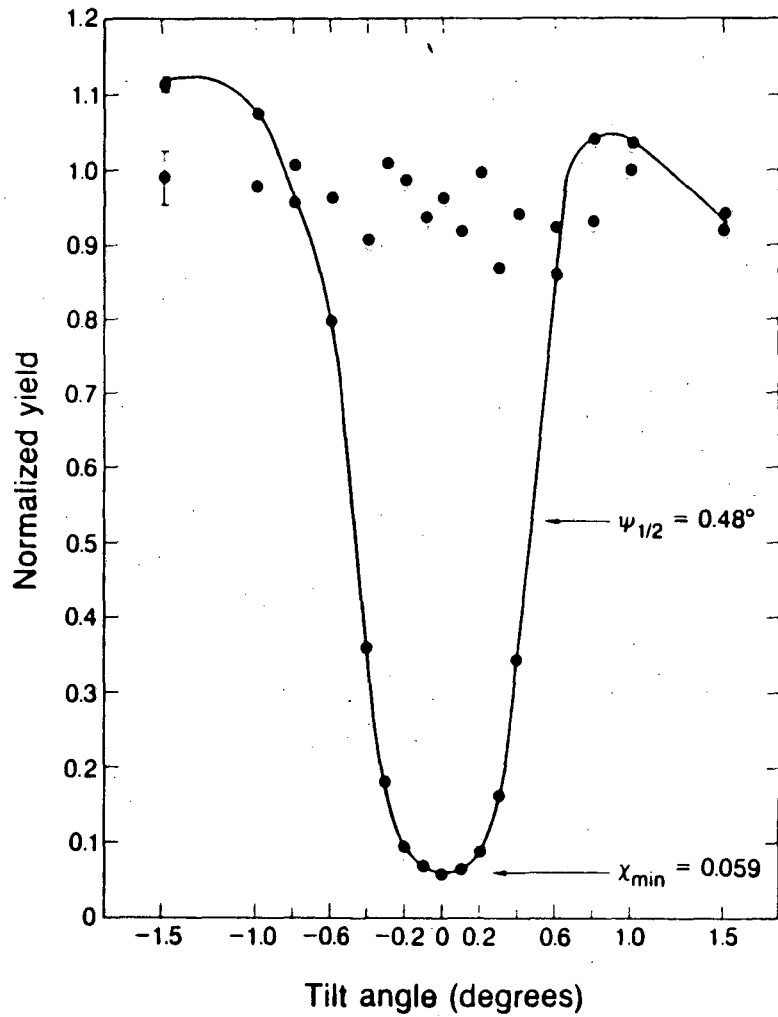


XBL 847-10744

Figure 14. Random and $\langle 100 \rangle$ spectra showing silicon, cobalt, and gold.

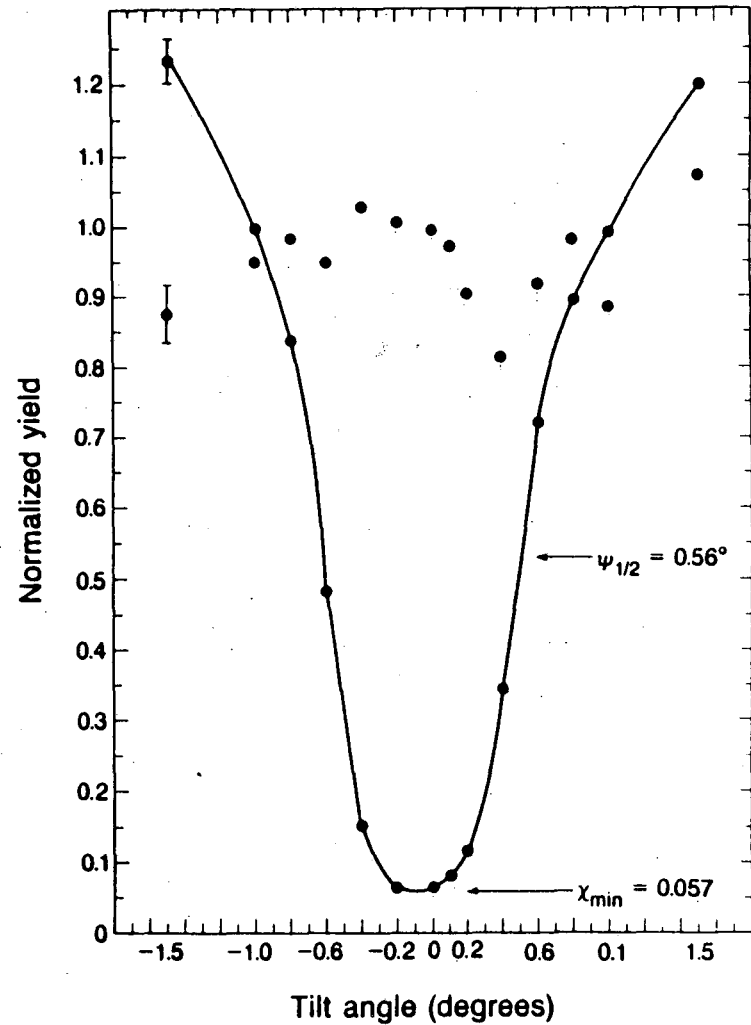
translated to a fresh area and an abbreviated angular scan consisting of only three points prior to the aligned position was obtained. This scan showed no significant difference from the original scan and the possibility that the negative result was due to a beam effect was ruled out. Although this data is sufficient to indicate the lack of a preferred site, a $\langle 110 \rangle$ angular scan was also obtained and is shown in Figure 16. This data was taken at a beam energy of 1.75 MeV and 8 μC

doses. Again, the cobalt yield shows no dependence on tilt angle. The scattering of the data points is somewhat larger in this case due to an increasing problem in resolution. Since the cobalt was on the backside of the membrane, as the membrane was tilted 45° to the $\langle 110 \rangle$ position the beam lost more energy before striking the cobalt. Thus, the cobalt signal moved closer to the silicon edge and was not as well separated.



XBL 847-10742

Figure 15. Cobalt on silicon: <100> angular scan.



XBL 847-10741

Figure 16. Cobalt on silicon: <110> angular scan.

3.4 Discussion

The initial data obtained one month after preparation of the sample indicated the existence of a preferred site for cobalt at the silicon surface. It is impossible to determine what type of site it may be (ie. substitutional or interstitial) as data from only one orientation was obtained. An estimate of the fraction of cobalt atoms located on preferred sites can be obtained from the relation:²⁷

$$\frac{1 - x_{\min}^{\text{impurity}}}{1 - x_{\min}^{\text{host}}}$$

Approximately $16 \pm 5\%$ or $7 \pm 2 \times 10^{14}$ cobalt atoms/cm² were located on preferred sites. The uncertainty in this number is determined by the counting statistics of the experiment.

These observations compare favorably with the thorough lattice location experiment of Cheung and Mayer¹⁹ on the Ni-Si system. In that study membranes with a coverage of 9×10^{15} nickel atoms/cm² were prepared under similar conditions as in this work. A 23% decrease in the yield from the nickel atoms was observed in the $\langle 100 \rangle$ and $\langle 111 \rangle$ directions while no dip was seen in the $\langle 110 \rangle$ direction. Planar channeling results were also obtained. The data indicated that 23% or 2.1×10^{15} Ni atoms/cm² occupied the tetrahedral interstitial site. It is not unlikely that similar results would be obtained for these two systems as both cobalt and nickel are transition metals with partially filled d-orbitals and are located next to each other on the periodic chart. Furthermore, both elements form silicides including epitaxial disilicides.²⁸

The data obtained seven months after the samples were prepared showed no evidence of a preferred site for cobalt. What might account for a change in the position of the cobalt atoms, and is there any experimental evidence of a change in the samples? Room temperature oxidation of the membrane is certainly a possible way in which the surface of the sample could change and with it the location of the cobalt atoms. Usually one cannot study the scattering information from elements lighter than the substrate, but in this case it is possible because the substrate is a thin membrane. The oxygen signal appears at lower energies than the low energy edge of the silicon membrane. Since the energy of the beam at the back side of the membrane differs from that incident on the front side, the oxygen signal coming from each side will be separated in energy also. However, it is not possible to measure the oxygen signal from the side which also has the cobalt on it in the case of the data taken after one month. In that case the oxygen signal from the side where cobalt atoms are present overlaps with the carbon signal from the front surface. It is possible to compare the amount of oxygen present on the front, cobalt-free sides for both sets of data. Also, in the case of the data taken after seven months, one can compare the amount of oxide on the two sides of the membrane because a different beam energy was used in that experiment. Careful examination of representative spectra from each run showed that the amount of oxide increased during the six month time period by a factor of 1.7 or from approximately 7×10^{15} oxygen atoms/cm² to 1×10^{16} oxygen atoms/cm². This corresponds to an increase of approximately 10 Å of

oxide.²⁹ In the case of the data taken after seven months, there is an equal amount of oxide at the front and back surfaces within experimental error. Hence, it is reasonable to expect that an additional 10 Å of oxide was formed on the surface where cobalt atoms were present. The amount of cobalt atoms on preferred sites was originally found to be 7×10^{14} atoms/cm² which is very close to one monolayer of <100> silicon atoms ($= 6.8 \times 10^{14}$ Si atoms/cm²).³⁰ If these atoms are occupying sites in the first few monolayers on the silicon surface, it is reasonable that the environment of the cobalt atoms was completely changed by room temperature oxidation between experiments.

4. Conclusions

Equipment modifications have been made to the LBL RBS facility to enhance the performance of channeling experiments. Additionally, an investigation of the lattice location of cobalt on the (100) silicon surface was pursued as an application of the channeling technique. A summary of the results and conclusions are given below:

- A significant improvement has been achieved at the LBL RBS facility for performing channeling experiments. The important equipment modifications include the addition of a new, high precision goniometer and improvement of beam collimation. These changes allow one to align a single crystal at a variety of orientations and carry out precise angular scans at each orientation.
- Angular scans about the $\langle 100 \rangle$, $\langle 110 \rangle$, and $\langle 111 \rangle$ directions of a silicon crystal demonstrate the improved channeling capability. The critical angles of these scans compared very well with known values while the values of the minimum yield were consistent with known values considering the effect of beam damage.
- A preferred site for (16% or 7×10^{14} atoms/cm²) of the cobalt atoms deposited on the Si(100) surface was indicated by preliminary channeling results using the original goniometer. However, no specific lattice site can be

identified as it was not possible to obtain angular scans at orientations other than the cut orientation of the crystal. The data is qualitatively consistent with either a substitutional or an interstitial site.

- Using the new goniometer, angular scans about the $\langle 100 \rangle$ and $\langle 110 \rangle$ directions were obtained on the same sample six months later. The data indicates that cobalt atoms occupy no preferred site with respect to the silicon lattice.
- It is believed that the room temperature oxidation of the sample between experiments altered the position of the cobalt atoms at the silicon surface. Experimental data showed that 10 Å of oxide formed during the time between the two experiments.

6. References

1. W. K. Chu, J. W. Mayer, and M. A. Nicolet, Backscattering Spectrometry, (Academic Press, New York, 1978), p. 21.
2. L. C. Feldman, J. W. Mayer, and S. T. Picraux, Materials Analysis By Ion Channeling, (Academic Press, New York, 1982).
3. W. Brandt, Sci. Am. 218, 90 (1968).
4. S. T. Picraux, New Uses of Ion Accelerators, J. F. Ziegler, ed., (Plenum Press, New York, 1975), p. 229.
5. D. K. Sadana, M. Strathman, J. Washburn, and G. R. Booker, J. Appl. Phys. 51, 5718 (1980).
6. D. K. Sadana, M. Strathman, J. Washburn, C. W. Magee, M. Maenpaa, and G. R. Booker, Appl. Phys. Lett 37, 615 (1980).
7. D. K. Sadana, M. Strathman, J. Washburn, and G. R. Booker, J. Appl. Phys. 52, 744 (1981).
8. D. K. Sadana and J. Washburn, Phys. Rev. B 24, 3626 (1981).
9. S. T. Picraux, E. Rimini, G. Foti, and S. U. Compisano, Phys. Rev. B 18, 2078 (1978).
10. Feldman, Mayer, and Picraux, op. cit., p. 88.
11. J. H. Barrett, Phys. Rev. B 3, 1527 (1971).
12. B. R. Appleton and G. Foti, Ion Beam Handbook for Material Analysis, J. W. Mayer and E. Rimini, eds. (Academic Press, New York, 1977), p. 69.
13. S. P. Murarka, Silicides For VLSI Applications, (Academic Press, New York, 1983), p. 1.

14. I. Lindau, P. W. Chye, C. M. Garner, P. Pianetta, C. Y. Su, and W. E. Spicer, *J. Vac. Sci. Technol.* 15, 1332 (1978).
15. S. Krawczyk and P. Viktorovitch, *Thin Solid Films* 111, 1 (1984).
16. G. Ottaviani, *J. Vac. Sci. Technol.* 18, 924 (1981).
17. G. Ottaviani, K. N. Tu, and J. W. Mayer, *Phys. Rev. Lett.* 44, 284 (1980).
18. K. N. Tu, *Appl. Phys. Lett.* 27, 221 (1975).
19. N. W. Cheung and J. W. Mayer, *Phys. Rev. Lett* 46, 671 (1981).
20. R. M. Walser and R. W. Bené, *Appl. Phys. Lett.* 28, 624 (1976).
21. R. W. Bené, R. M. Walser, G. S. Lee, and K. C. Chen, *J. Vac. Sci. Technol.* 17, 911 (1980).
22. J. F. Van Der Veen, R. M. Tromp, R. G. Smeenk, and F. W. Saris, *Surf. Sci.* 82, 468 (1979).
23. N. W. Cheung, *Rev. Sci. Instrum.* 51, 1212 (1980).
24. E. Rimini, J. Haskell, and J. W. Mayer, *Appl. Phys. Lett.* 20, 237 (1972).
25. E. Kotai, T. Lohner, A. Manuaba, G. Mezey, R. Coussement, I. Dezsi, and G. Langouche, *Radiat. Eff.* 47, 153 (1980).
26. N. W. Cheung, R. J. Culbertson, L. C. Feldman, P. J. Silverman, K. W. West, and J. W. Mayer, *Phys. Rev. Lett.* 45, 120 (1980).
27. Feldman, Mayer, and Picraux, *op. cit.*, p. 59.
28. Murarka, *op. cit.*, p. 172.

29. L. C. Feldman, I. Stensgaard, P. J. Silverman, and T. E. Jackman, The Physics of SiO₂ and its Interfaces, S. T. Pantelides, ed., (Pergamon Press, New York 1978), p. 344.
30. N. W. Cheung, P. J. Grunthaner, F. J. Grunthaner, J. W. Mayer, and B. M. Ullrich, J. Vac. Sci. Technol. 18, 917 (1981).
31. E. R. Weber, Appl. Phys. A 30, 1 (1983).
32. W. Bergholz and W. Schroder, Phys. Stat. Sol. (a) 49, 489 (1978).
33. W. Bergholz, J. Phys. D 14, 1099 (1981)..

This report was done with support from the Department of Energy. Any conclusions or opinions expressed in this report represent solely those of the author(s) and not necessarily those of The Regents of the University of California, the Lawrence Berkeley Laboratory or the Department of Energy.

Reference to a company or product name does not imply approval or recommendation of the product by the University of California or the U.S. Department of Energy to the exclusion of others that may be suitable.

TECHNICAL INFORMATION DEPARTMENT
LAWRENCE BERKELEY LABORATORY
UNIVERSITY OF CALIFORNIA
BERKELEY, CALIFORNIA 94720